Original Research

Microstructure, phase stability and mechanical properties of Nb–Ni–Ti–Co–Zr and Nb–Ni–Ti–Co–Zr–Hf high entropy alloys

Zhidong Han, Xue Liu, Shaofan Zhao, Yang Shao, Jinfeng Li, Kefu Yao*

School of Materials Science and Engineering, Tsinghua University, Beijing 100084, China

Abstract

Owning to their excellent thermal stability and high strength at elevated temperature, high entropy alloys (HEAs) possess great potential for the application in aviation and aerospace fields. In present work, two novel Nb–Ni–Ti–Co–Zr and Nb–Ni–Ti–Co–Zr–Hf HEAs were prepared by arc melting and copper mold suction-casting method. The microstructure, phase stability, mechanical properties at room temperature and elevated temperature of the two HEAs were studied. Both of the HEAs possess high yield stress at room temperature, especially for the Nb–Ni–Ti–Co–Zr (with 2331 Mpa). In addition, the Nb–Ni–Ti–Co–Zr HEA exhibited high yield stress of 564 Mpa at elevated temperature of 800 °C and large compressive plastic strain (more than 50% at 800 °C). Nb–Ni–Ti–Co–Zr–Hf alloy showed new phase precipitation at 800 °C, whereas the structure of Nb–Ni–Ti–Co–Zr was more stable, which is one of the reason why it possesses high strength at room temperature and elevated temperature. The high temperature properties of the Nb–Ni–Ti–Co–Zr HEA make it promising for high temperature application.
© 2015 The Authors. Production and hosting by Elsevier B.V. on behalf of Chinese Materials Research Society. This is an open access article under the CC BY-NC-ND license (http://creativecommons.org/licenses/by-nc-nd/4.0/).

Keywords: High entropy alloy; Mechanical property; Microstructure, Stability

1. Introduction

High entropy alloys (HEAs), which contain at least 5 components in equiatomic or near-equiatomic ratio, have been considered as a new material in recent years [1–4]. It is known that the high mixing entropy could decrease the Gibbs free energy and result in the formation of solid solution phase of HEAs. Due to the high entropy and their complex microstructure in the multi-elements alloys, HEAs exhibit many attractive properties, such as high strength at both cryogenic temperatures [5–7] and high temperatures [8–12], strong corrosion resistance [13,14], outstanding wear resistance [15,16], excellent magnetic properties [17] and good glass-forming ability [18-19].

In particularly, the refractory high entropy alloys (HEAs) possess dramatic mechanical properties at high temperatures due to their high meting temperature and strong solid solution strengthening, and possess very high yield strength ($\sigma_{0.2}$) in the temperature range from 20 °C to 1000 °C. Although there are several refractory HEA systems with a simple solid solution structure, including Nb–Ta–Mo–W [10,11], Nb–Ti–Zr [8,12,20–24] and Nb–Ti–V–Al [25], have been successfully developed, the components of the reported refractory HEAs are limited in Nb, Ta, V, W, Ti, Zr, Hf and Al. Thus, developing refractory HEAs with other elements is of importance.

Since Ni-based and Co-based superalloys have been wildly applied [26,27] due to their excellent mechanical properties at elevated temperature, Ni and Co elements could be served as alloying elements in the refractory HEAs. In present work, by selecting Ni, Co, and the commonly used constituent elements such as Nb, Ti, Zr and Hf in refractory HEAs, two new refractory HEAs of $Nb_{20}Ni_{20}Ti_{20}Co_{20}Zr_{20}$ and $Nb_{16.7}Ni_{16.7}Ti_{16.7}Co_{16.7}Zr_{16.7}Hf_{16.7}$ were developed. The structural stability, mechanical properties at both room temperature and elevated temperatures have been investigated.

*Corresponding author. Tel.: +86 10 62772292; fax: +86 10 62771160.
E-mail address: kfyao@tsinghua.edu.cn (K. Yao).

2. Experimental procedures

The $Nb_{20}Ni_{20}Ti_{20}Co_{20}Zr_{20}$ and $Nb_{16.7}Ni_{16.7}Ti_{16.7}Co_{16.7}$ $Zr_{16.7}Hf_{16.7}$ HEAs in equiatomic ratio were prepared by vacuum arc melting of the mixtures of the metals in a Ti-gettered pure argon atmosphere. The purities of Nb, Ni, Co and Ti are over 99.9 mass%, and the purities of Zr and Hf are over 99.2 mass%. Each ingot was re-melted at least five times to ensure the compositional homogeneity. Then cylindrical rods were prepared by copper mold suction casting. The structure of the as-cast rods and anneal samples was characterized by Rigaku D/max-RB X-ray diffraction (XRD) using a Cu Kα radiation. To measure the room temperature mechanical properties of the alloys, the compression tests were performed on WDW-50 testing machine at a strain rate of $4 \times 10^{-4} \, s^{-1}$. The samples were cut out from the as-cast $\phi 3$ mm rods with gage aspect ratio of 2:1. The elevated temperature compression tests were carried out with Gleeble3500 thermal simulator at a strain of $1 \times 10^{-3} \, s^{-1}$ using samples with a dimension of $\phi 6$ mm $\times 9$ mm. The fractured samples were examined by Quanta 200 FEG scanning electron microscope (SEM). The hardness and elastic constants of the novel HEAs were measured by MH-3 vickers hardness tester and Teclab resonance ultrasonic spectrometer, respectively.

3. Results and discussions

Fig. 1a shows the XRD spectrum of the as-cast $Nb_{20}Ni_{20}Ti_{20}Co_{20}Zr_{20}$ alloy sample. Two body-centered cubic (BCC) phases with lattice constants of 3.14 Å and 3.33 Å were indexed., The XRD spectrum of the annealed $Nb_{20}Ni_{20}Ti_{20}Co_{20}Zr_{20}$ alloy sample after annealed at 800 °C for 1 h is shown in Fig. 1b, where the characteristic peaks are nearly the same as those in the XRD spectrum of as-cast sample. The indexing of the XRD spectrum confirmed that the annealed sample was still consisted of two BCC phases with lattice constants of 3.14 Å and 3.33 Å. Thus, the $Nb_{20}Ni_{20}Ti_{20}Co_{20}Zr_{20}$ alloy possesses excellent structural stability below 800 °C.

Fig. 1c shows the XRD spectrum of the as-cast $Nb_{16.7}Ni_{16.7}Ti_{16.7}Co_{16.7}Zr_{16.7}Hf_{16.7}$ HEA sample, where a BCC crystal structure, a faced-centered cubic (FCC) crystal structure and a NbNi intermetallic phase were indentified. The lattice constants of the BCC and FCC phases were measured to be 4.48 Å ($a'1$) and 4.74 Å ($a'2$), respectively. By comparing the XRD results of the as-cast $Nb_{20}Ni_{20}Ti_{20}Co_{20}Zr_{20}$ and $Nb_{16.7}Ni_{16.7}Ti_{16.7}Co_{16.7}Zr_{16.7}Hf_{16.7}$ alloys, it could be found that the addition of Hf can promote the phase transformation from BCC phase to FCC phase. Similar FCC to BCC phase transformation phenomenon has been observed in $CuCrFeNiCu_{1-x}Al_x$ HEAs when increase the Al content [28]. The phase transformation phenomenon was reported to be closely related to the great lattice constant difference between the Al and other elements.

After annealing at 800 °C for one hour, a new $NbHf_2$ phase was observed in the XRD spectrum of the annealed $Nb_{16.7}Ni_{16.7}Ti_{16.7}Co_{16.7}Zr_{16.7}Hf_{16.7}$ HEA sample, as shown in Fig. 1d. The precipitation of new phase might be on account of

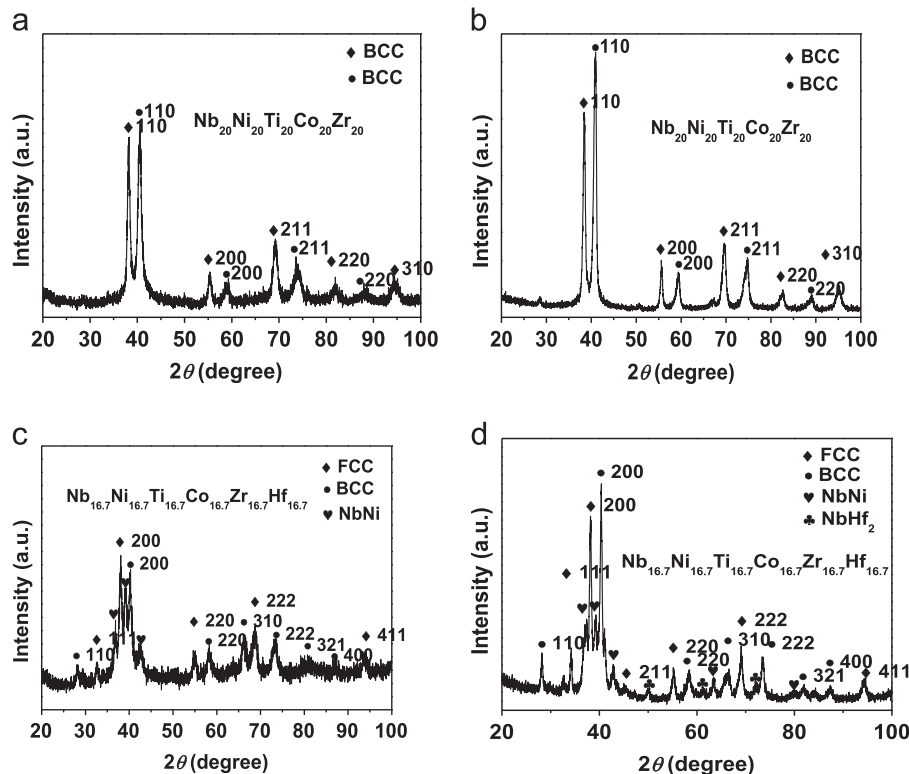Fig. 1. XRD patterns of (a) the as-cast and (b) the annealed $Nb_{20}Ni_{20}Ti_{20}Co_{20}Zr_{20}$ HEA samples, and (c) the as-cast and (d) the annealed $Nb_{16.7}Ni_{16.7}Ti_{16.7}Co_{16.7}Zr_{16.7}Hf_{16.7}$ HEA samples.

the obviously increased lattice constants in the $Nb_{20}Ni_{20}Ti_{20}Co_{20}Zr_{20}$ HEA, which could promote the migration of Ni and Co elements with relatively low melt point and small atom radius.(Table 1)

The optical microscopic images of the as-cast and annealed HEAs are shown in Fig. 2, where all the samples exhibited dendritic structure. The grain size of the as-cast $Nb_{20}Ni_{20}Ti_{20}Co_{20}Zr_{20}$ HEA sample was somehow non-uniform, and the average grain size was $\sim 5\,\mu m$. The as-cast $Nb_{16.7}Ni_{16.7}Ti_{16.7}Co_{16.7}Zr_{16.7}Hf_{16.7}$ HEA sample possessed a similar grain size (as shown in Fig. 2c). After annealing, the grain sizes of both the two HEAs didn't change, indicating that no obvious grain growth occurred during the annealing process.

The micro-hardness of the two as-cast and annealed alloys was measured by MH-3 vickers hardness tests, and the values of hardness are shown in Table 2. The hardness of the as-cast $Nb_{20}Ni_{20}Ti_{20}Co_{20}Zr_{20}$ HEA was 527.3 ± 6.9. After annealing, the hardness of the annealed sample decreased to 489.2 ± 25.3, which might be resulted by the stress relief during the annealing process. The hardness of the as-cast $Nb_{16.7}Ni_{16.7}Ti_{16.7}Co_{16.7}Zr_{16.7}Hf_{16.7}$ HEA was 515.5 ± 11.2. While after annealing, the hardness of the sample slightly increased to 520.1 ± 2.0, which could be associated with the formation of the $NbHf_2$.

The elastic constants of the two HEAs were also investigated. The $Nb_{20}Ni_{20}Ti_{20}Co_{20}Zr_{20}$ HEA possessed a bulk modulus of 185 GPa, a shear modulus of 90 GPa, a Youngs

Table 1

The crystalline phase and crystalline lattices of the $Nb_{20}Ni_{20}Ti_{20}Co_{20}Zr_{20}$ and $Nb_{16.7}Ni_{16.7}Co_{16.7}Zr_{16.7}Hf_{16.7}$ HEAs.

Components	Lattice constants of the BCC/FCC phases (nm)	
$Nb_{20}Ni_{20}Ti_{20}Co_{20}Zr_{20}$	0.314 (FCC)	0.333 (FCC)
$Nb_{16.7}Ni_{16.7}Ti_{16.7}Co_{16.7}Zr_{16.7}Hf_{16.7}$	0.448 (BCC)	0.474 (FCC)

Table 2

Vickers microhardness values of the $Nb_{20}Ni_{20}Ti_{20}Co_{20}Zr_{20}$ and $Nb_{16.7}Ni_{16.7}Ti_{16.7}Co_{16.7}Zr_{16.7}Hf_{16.7}$ HEAs.

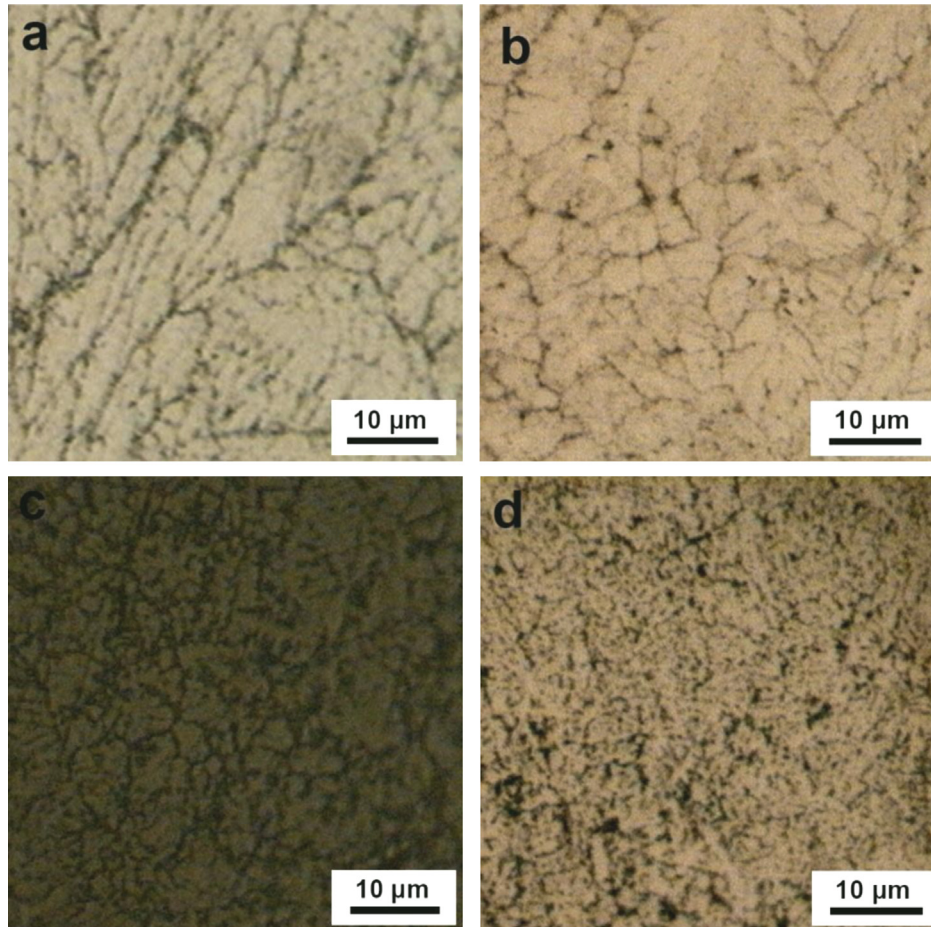| Sample	$Nb_{20}Ni_{20}Ti_{20}Co_{20}Zr_{20}$		$Nb_{16.7}Ni_{16.7}Ti_{16.7}Co_{16.7}Zr_{16.7}Hf_{16.7}$	
	As-cast	Annealed	As-cast	Annealed
Hardness (HV)	527.3 ± 6.9	489.2 ± 25.3	515.5 ± 11.2	520.1 ± 2.0

Fig. 2. Microstructures of (a) the as-cast and (b) the annealed $Nb_{20}Ni_{20}Ti_{20}Co_{20}Zr_{20}$ HEAs, and (c) the as-cast and (d) the annealed $Nb_{16.7}Ni_{16.7}Ti_{16.7}Co_{16.7}Zr_{16.7}Hf_{16.7}$ HEAs.

modulus of 234 GPa and Possion's ratio of 0.290. The $Nb_{16.7}Ni_{16.7}Ti_{16.7}Co_{16.7}Zr_{16.7}Hf_{16.7}$ HEA possessed a bulk modulus of 170 GPa, a shear modulus of 110 GPa, a Youngs modulus of 272 GPa and a Possion's ratio of 0.233.

Fig. 3 shows the stress–strain curves of the $Nb_{20}Ni_{20}Ti_{20}Co_{20}Zr_{20}$ and $Nb_{16.7}Ni_{16.7}Ti_{16.7}Co_{16.7}Zr_{16.7}Hf_{16.7}$ HEAs. The $\sigma_{0.2}$ value of the $Nb_{20}Ni_{20}Ti_{20}Co_{20}Zr_{20}$ HEA is as high as 2331 Mpa, and the fracture occurred at the peak stress (σ_u) of 2504 Mpa. The high stress of the $Nb_{20}Ni_{20}Ti_{20}Co_{20}Zr_{20}$ HEA may be due to its BCC structures with relatively high strength and the small grain size, which both can promote the strength of the crystalline materials. In addition, the strong bonding inherited from the fractory elements and the high solution hardening effect of the matrix can also enhance the strength of the HEA.

The $\sigma_{0.2}$ value of the $Nb_{16.7}Ni_{16.7}Ti_{16.7}Co_{16.7}Zr_{16.7}Hf_{16.7}$ HEA is of 1469 Mpa, which is much lower than that of the $Nb_{20}Ni_{20}Ti_{20}Co_{20}Zr_{20}$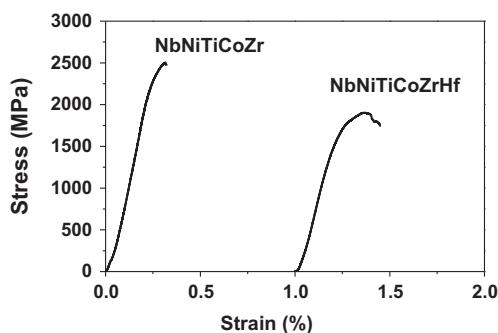 HEA. This low compressive strength might be partly caused by the existence of FCC phase with relatively low strength. But the $Nb_{16.7}Ni_{16.7}Ti_{16.7}Co_{16.7}Zr_{16.7}Hf_{16.7}$ HEA exhibits slightly better plasticity, as shown in Fig. 3.

SEM images of the fracture surfaces of the $Nb_{20}Ni_{20}Ti_{20}Co_{20}Zr_{20}$ and $Nb_{16.7}Ni_{16.7}Ti_{16.7}Co_{16.7}Zr_{16.7}Hf_{16.7}$ HEAs are shown in Fig. 4. It could be found that both of the two HEA samples exhibited a typical shear fracture mode at room temperature with a shearing angle of $\sim 45^o$, as shown in Fig. 4a and c. Flat facets, river-pattern markings and cleavage feathers were noticed in the higher magnification images shown in Fig. 4b and d, indicating the characteristics of the quasi-cleavage fracture.

The good phase stability at high temperature is strongly correlated to the superior mechanical properties at elevated temperature. Thus, in present study, only the $Nb_{20}Ni_{20}Ti_{20}Co_{20}Zr_{20}$ HEA, which possess both higher strength at room temperature and better phase stability, was employed to explore its mechanical properties at 600–1000 °C. The compression stress–strain curves of the $Nb_{20}Ni_{20}Ti_{20}Co_{20}Zr_{20}$ HEA at elevated temperatures were shown in Fig. 5. The values of the $\sigma_{0.2}$ and σ_u at different temperatures were listed in Table 3. The $\sigma_{0.2}$ value of the $Nb_{20}Ni_{20}Ti_{20}Co_{20}Zr_{20}$ HEA was 1385 Mpa at 600 °C, and the brittle fracture occurred at σ_u of 1566 Mpa. As the temperature increased to 700 °C, the $\sigma_{0.2}$ value decreased to 668 Mpa and a brittle to ductile transition occurred. The brittle to ductile transition temperature (BDTT) could be clearly observed in the temperature ranges from 600 °C to 700 °C. All the fracture strain (ε) values of the $Nb_{20}Ni_{20}Ti_{20}Co_{20}Zr_{20}$ HEA in the temperature range of 700–1000 °C were more than 50%. With the increasing

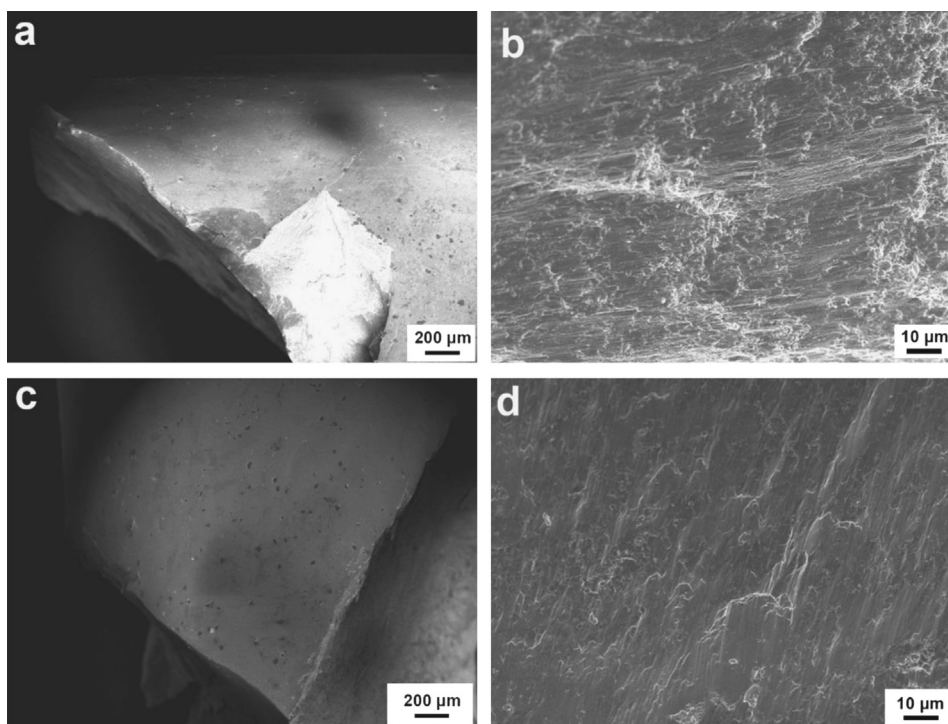Fig. 3. Compressive stress–strain curves of the $Nb_{20}Ni_{20}Ti_{20}Co_{20}Zr_{20}$ and $Nb_{16.7}Ni_{16.7}Ti_{16.7}Co_{16.7}Zr_{16.7}Hf_{16.7}$ HEAs at room temperature.

Fig. 4. SEM images of the fracture surfaces of the $Nb_{20}Ni_{20}Ti_{20}Co_{20}Zr_{20}$ and $Nb_{16.7}Ni_{16.7}Ti_{16.7}Co_{16.7}Zr_{16.7}Hf_{16.7}$ HEAs subjected to a compressive fracture.
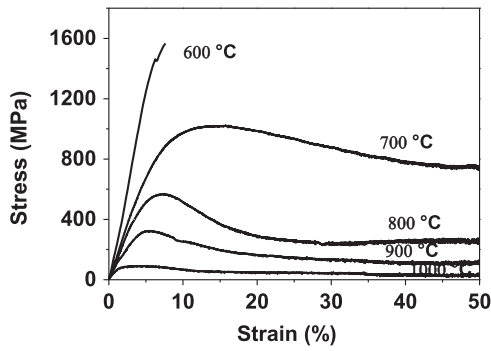
Fig. 5. Compressive engineering stress–strain curves for the $Nb_{20}Ni_{20}Ti_{20}Co_{20}Zr_{20}$ HEA obtained at elevated temperatures.

Table 3
The $\sigma_{0.2}$ and σ_u values of the $Nb_{20}Ni_{20}Ti_{20}Co_{20}Zr_{20}$ HEA at different temperatures.

Temperature (°C)	$\sigma_{0.2}$ (MPa)	$\sigma_{0.2}$ (MPa)
600	1385	1566
700	668	1021
800	427	567
900	213	324
1000	60	91

temperature, the $\sigma_{0.2}$ value of the $Nb_{20}Ni_{20}Ti_{20}Co_{20}Zr_{20}$ HEA decreased gradually. When the temperature raised to 1000 °C, the $\sigma_{0.2}$ value of the $Nb_{20}Ni_{20}Ti_{20}Co_{20}Zr_{20}$ HEA dropped to 60 Mpa.

The decreased $\sigma_{0.2}$ from 1385 Mpa at 600 °C to 668 Mpa at 700 °C might own to the brittle to ductile transition. However, it is known that the weakening of chemical bond between metal elements generally happened at temperatures above about 0.5–0.6 times of the absolutely melt point T_m (they are 611–787 °C for Co, and 590–762 °C for Ni, respectively). Thus, the significantly decreased of $\sigma_{0.2}$ at the temperature above 700 °C might result from the weakening of chemical bond of Co and Ni elements.

4. Conclusions

Two new HEAs of $Nb_{20}Ni_{20}Ti_{20}Co_{20}Zr_{20}$ and $Nb_{16.7}Ni_{16.7}Ti_{16.7}Co_{16.7}Zr_{16.7}Hf_{16.7}$ had been developed. The $Nb_{20}Ni_{20}Ti_{20}Co_{20}Zr_{20}$ HEA is consisted by two BCC phases. With Hf addition, a BCC phase, a FCC phase and a NbNi intermetallic phase were indentified in the $Nb_{16.7}Ni_{16.7}Ti_{16.7}Co_{16.7}Zr_{16.7}Hf_{16.7}$ HEA. The $Nb_{20}Ni_{20}Ti_{20}Co_{20}Zr_{20}$ HEA possesses excellent structural stability, and exhibits high yield strength from 20 °C to 800 °C and large strain above 700 °C, which makes it promising for application at high temperature.

References

[1] P.K. Huang, J.W. Yeh, T.T. Shun, S.K. Chen, Adv. Eng. Mater. 6 (1–2) (2004) 74–78.
[2] J.W. Yeh, Ann. Chim. Sci. Mat. 31 (6) (2006) 633–648.
[3] J.W. Yeh, S.K. Chen, S.J. Lin, J.Y. Gan, T.S. Chin, T.T. Shun, C.H. Tsau, S.Y. Chang, Adv. Eng. Mater. 6 (5) (2004) 299–303 2004.
[4] Y. Zhang, Y.J. Zhou, J.P. Lin, G.L. Chen, P.K. Liaw, Adv. Eng. Mater. 10 (6) (2008) 534–538.
[5] B. Gludovatz, A. Hohenwarter, D. Catoor, E.H. Chang, E.P. George, R.O. Ritchie, Science 345 (2014) 1153–1158.
[6] A. Gali, E.P. George, Intermetallics 39 (2013) 74–78.
[7] M.A. Laktionova, E.D. Tabchnikova, Z. Tang, P.K. Liaw, Low Temp. Phys. 39 (2013) 630–632.
[8] O.N. Senkov, J.M. Scott, S.V. Senkova, F. Meisenkothen, D.B. Miracle, C.F. Woodward, J. Mater. Sci. 47 (2012) 4062–4074.
[9] O.N. Senkov, S.V. Senkova, D.B. Miracle, C. Woodward, Mater. Sci. Eng. A 565 (2013) 51–62.
[10] O.N. Senkov, G.B. Wilks, J.M. Scott, D.B. Miracle, Intermetallics 19 (2011) 698–706.
[11] O.N. Senkov, C. Woodward, D.B. Miracle, JOM 66 (2014) 2030–2042.
[12] Y.D. Wu, Y.H. Cai, T. Wang, J.J. Si, J. Zhu, Y.D. Wang, X.D. Hui, Mater. Lett. 130 (2014) 277–280.
[13] J. Li, X. Yang, R. Zhu, Y. Zhang, Metals 4 (2014) 597–608.
[14] V. Soare, D. Mitrica, I. Constantin, G. Popescu, I. Csaki, M. Tarcolea, I. Carcea, Metall. Mater. Trans. A 46A (2014) 1468–1473.
[15] M.H. Chuang, M.H. Tsai, W.R. Wang, S.J. Lin, J.W. Yeh, Acta Mater. 59 (2011) 6308–6317.
[16] C.Y. Hsu, J.W. Yeh, S.K. Chen, T.T. Shun, Metall. Mater. Trans. A 35A (2004) 1465–1469.
[17] C.D. Gómez-Esparza, F.J. Baldenebro-López, C.R. Santillán-Rodríguez, I. Estrada-Guel, J.A. Matutes-Aquino, J.M. Herrera-Ramírez, R. Martínez-Sánchez, J. Alloy. Compd. 615 (2014) S317–S323.
[18] H.Y. Ding, Y. Shao, P. Gong, J.F. Li, K.F. Yao, Mater. Lett. 125 (2014) 151–153.
[19] H.Y. Ding, K.F. Yao, J Non-Cryst. Solids 364 (2013) 9–12.
[20] O.N. Senkov, J.M. Scott, S.V. Senkova, D.B. Miracle, C.F. Woodward, J. Alloy. Compd. 509 (2011) 6043–6048.
[21] J.P. Couzinié, G. Dirras, L. Perrière, T. Chauveau, E. Leroy, Y. Champion, I. Guillot, Mater. Lett. 126 (2014) 285–287.
[22] O.N. Senkov, S.V. Senkova, C. Woodward, D.B. Miracle, Acta Mater. 61 (2013) 1545–1557.
[23] É. Fazakas, V. Zadorozhnyy, L.K. Varga, A. Inoue, D.V. Louzguine-Luzgin, F. Tian, L. Vitos, Int. J. Refract. Met. Hard Mater. 47 (2014) 131–138.
[24] M.G. Poletti, G. Fiore, B.A. Szost, L. Battezzati, J. Alloy. Compd. 620 (2015) 283–288.
[25] N.D. Stepanov, D.G. Shaysultanov, G.A. Salishchev, M.A. Tikhonovsky, Mater. Lett. 142 (2015) 153–155.
[26] T.M. Pollock, S. Tin, J. Propuls. Power 22 (2006) 361–374.
[27] D. Coutsouradis, A. Davin, M. Lamberigts, Mater. Sci. Eng. 88 (1987) 11–19.
[28] Y.J. Zhou, Y. Zhang, F.J. Wang, G.L. Chen, Appl. Phys. Lett. 92 (2008) 241917.